A Global View of Martian Surface Compositions from MGS-TES

Joshua L. Bandfield, *et al.*

Science **287**, 1626 (2000);
DOI: 10.1126/science.287.5458.1626

41. K.-F. Wang, Y.-L. Zhang, H. Jian, *Chin. Sci. Bull.* **36**, 1721 (1991).
42. Z. Zhu *et al.*, *Quat. Sci.* **8**, 276 (1995).
43. C. C. Swisher Jr. *et al.*, *Science* **263**, 1118 (1994).
44. N. Toth and K. Schick, in *Tools, Language and Cognition in Human Evolution*, K. R. Gibson and T. Ingold, Eds. (Cambridge Univ. Press, Cambridge, 1992), pp. 346–362.
45. P. Teilhard de Chardin, C. C. Young, W. C. Pei, H. C. Chang, *Bull. Geol. Soc. China* **14**, 179 (1935).
46. K. Hutterer, in *Sunda and Sahul: Prehistoric Studies in Southeast Asia, Melanesia and Australia*, J. Allen, J. Golson, R. Jones, Eds. (Academic Press, New York, 1977), pp. 31–72.
47. G. G. Pope, in *The Palaeoenvironment of East Asia from the Mid-Tertiary*, J. S. Aigner, N. G. Jablonski, G. Taylor, D. Walker, P. Wang, Eds. (Centre of Asian Studies, Univ. of Hong Kong, Hong Kong, 1988), pp. 1097–1123.
48. H. Watanabe, *J. Anthropol. Archaeol.* **4**, 1 (1985).
49. J. D. Clark, *Trans. R. Soc. London Ser. B* **337**, 201 (1992).
50. K. Bai, thesis, University of California, Berkeley (1988).
51. T. Chen and S. Yuan, *Archaeometry* **30**, 59 (1988).
52. H. Kajiwara, S. Fujimura, T. Kamada, Y. Yokoyama, http://tfu-www.tfu.ac.jp/kenkyushitsu/kajiwara/KAJIWARA.html (1999).
53. W. Huang, *Quat. Res.* **28**, 237 (1989).
54. _____, J. Leng, X. Yuan, G. Xie, *Acta Anthropol. Sin.* **9**, 105 (1990).
55. S.-L. Guo, W. Huang, X.-H. Hao, B.-L. Chen, *Radiat. Meas.* **28**, 565 (1997).
56. W. Sharp and A. L. Deino, *Eos* **77**, F773 (1996).
57. G. A. Izett and J. D. Obradovich, *J. Geophys. Res.* **99**, 2925 (1992).
58. P. R. Renne *et al.*, *Chem. Geol.* **145**, 117 (1998).
59. D. A. Schneider, D. V. Kent, G. A. Mello, *Earth Planet. Sci. Lett.* **111**, 395 (1992).
60. B. S. Singer and M. S. Pringle, *Earth Planet. Sci. Lett.* **139**, 41 (1996).
61. R. Potts, unpublished data on Oldowan and Developed Oldowan sites.
62. P. Callow, in *Olduvai Gorge*, vol. 5, M. D. Leakey, Ed. (Cambridge Univ. Press, Cambridge, 1994), pp. 235–253.
63. P. R. Jones, in *Olduvai Gorge*, vol. 5, M. D. Leakey, Ed. (Cambridge Univ. Press, Cambridge, 1994), pp. 254–298.
64. M. N. Noll, thesis, University of Illinois, Urbana-Champaign (2000).
65. We thank the government of the Guangxi Zhuang Autonomous Region and the Chinese Academy of Sciences for permission to conduct the Bose basin research. Supported by funds from the Smithsonian Institution's Human Origins Program and Scholarly Studies Program, by Chinese Academy of Sciences grant SEPP 9812, by National Natural Science Foundation of China grant 49894176, and by NSF. We thank W. G. Melson and F. M. Hueber for analytical assistance, M. N. Noll for data on Olorgesailie LCTs, and A. K. Behrensmeyer and A. S. Brooks for helpful discussions.

17 December 1999; accepted 31 January 2000

REPORTS

A Global View of Martian Surface Compositions from MGS-TES

Joshua L. Bandfield,* Victoria E. Hamilton, Philip R. Christensen

Thermal Emission Spectrometer (TES) data from the Mars Global Surveyor (MGS) are used to determine compositions and distributions of martian low-albedo regions. Two surface spectral signatures are identified from low-albedo regions. Comparisons with spectra of terrestrial rock samples and deconvolution results indicate that the two compositions are a basaltic composition dominated by plagioclase feldspar and clinopyroxene and an andesitic composition dominated by plagioclase feldspar and volcanic glass. The distribution of the two compositions is split roughly along the planetary dichotomy. The basaltic composition is confined to older surfaces, and the more silicic composition is concentrated in the younger northern plains.

A major objective of the TES investigation is to determine and map the mineralogy of the martian surface in order to understand the formation and development of Mars. To understand present and past conditions on Mars, it is important to determine if the surface materials are, for example, volcanic, weathering products, or chemical precipitates. We demonstrate here that martian dark materials are volcanic and that they vary significantly across the planet. These findings can help lead to an understanding of planetary mechanisms such as the development of the martian crust, heat loss processes, bulk composition, magma differentiation, and source materials of the martian soil and dust.

Previous studies have developed the methodology for separating the surface and atmospheric components of the emission of Mars (*1*, *2*), allowing detailed analysis and interpretation of the surface composition (*3*, *4*) and atmospheric properties (*5*). The spectra of the martian surface match the spectra of rock samples and linear mixtures of minerals measured in the laboratory; there is no evidence for unusual particle size or environmental effects (*3, 4*). Atmospherically corrected TES spectra of the dark surface region of Terra Cimmeria can be matched to basalt, with a derived composition dominated by plagioclase and with lesser clinopyroxene. Analysis of TES spectra has also revealed the presence of a unique area of hematite mineralization in the equatorial Sinus Meridiani region (*4*). Here we present a global map of the petrologic and mineralogic composition of martian volcanic materials with the TES data acquired since the beginning of the MGS mapping mission (*6*).

Surface spectra were retrieved with surface atmosphere separation techniques (*1–3*). Two independent methods have been developed that provide nearly identical results (*7*) for the variety of surfaces presented here. The analysis presented here was performed with the deconvolution algorithm (*2*). Several surface locations were also selected for analysis with the radiative transfer algorithm (*2*) to check the consistency of the results derived from the deconvolution algorithm.

Atmospherically corrected surface emissivity spectra were analyzed with two methodologies. First, a direct comparison of martian surface spectra with laboratory thermal emission spectra of terrestrial rock samples can be used to provide a good estimate of bulk composition (*3*, *8–11*). However, this technique may be limited because surfaces may be mixtures of minerals that do not represent a single rock composition. In addition, it is difficult to obtain precise compositions with this technique because the number of possible realistic surface compositions is far greater than any rock library can account for.

A second, more quantitative technique is linear deconvolution of surface emissivity spectra using a spectral library of minerals (*11–14*). This technique takes advantage of the fact that a thermal infrared spectrum of a mixed mineral surface may be closely modeled with a linear combination of mineral spectra multiplied by their areal concentrations (*11–16*). Linear deconvolution of laboratory spectra may be used to retrieve the modal mineralogies of a variety of rock samples to within 5 to 10 volume % (5–10 vol. %) of optical modes (*11, 14*). The uncertainty for the martian TES spectra is somewhat higher than these laboratory studies (~10–15 vol. %) (*3, 14*) because the martian surface spectra were acquired at lower spectral resolution, have a more limited wavelength range, and have additional uncertainties due to the removal of atmospheric effects.

Spectra of mineral mixtures, such as rocks or TES observations, are often difficult to

Department of Geology, Arizona State University, Tempe, AZ 85287–1404, USA.

*To whom correspondence should be addressed. E-mail: joshband@asu.edu

analyze using simple comparisons with individual minerals. Absorption bands in silicates often overlap, and the fine-scale structure in an individual mineral spectrum combines linearly with other minerals to produce a more complex rock spectrum (*3*). However, deconvolution and direct comparisons allow minerals to be identified even though their individual spectral features may not be visibly distinct from the spectral features of other minerals present.

Surface spectra were retrieved from 25 locations. Data used for each location were selected based on low dust and water-ice opacities (<0.3 and <0.1, respectively), warm surface temperatures (>270 K), low emission angles (<30°), and low albedo (<0.15). Dark regions, which make up ~50% of the martian surface, were selected to minimize the spectral contributions due to globally homogeneous, fine-grained bright dust (*17*–*19*). Several dozen to several hundred spectra were selected and averaged together from each location, and the atmosphere was removed from each average spectrum with locally derived atmospheric dust and water-ice spectral shapes (*1*).

All of the selected surface spectral signatures are similar in that all surface spectral shapes contain broad absorptions in the ~800 to 1200 cm^{-1} (8 to 12 μm) and ~200 to 500 cm^{-1} (20 to 50 μm) wavenumber regions. The depth of the absorptions varies between ~0.04 and 0.09 in emissivity. Despite these gross similarities, differences exist among the spectral shapes that permit the spectra to be grouped into two components (Fig. 1). The first component contains a broad, slightly square-shaped absorption between ~800 and 1200 cm^{-1} and absorption through the ~200 to 500 cm^{-1} region. The ~200 to 500 cm^{-1} absorption has an overall negative slope with decreasing wavenumbers (increasing wavelength) and contains superimposed minor, narrow absorptions. This spectral shape is similar to that analyzed by Christensen *et al.* (*3*). A second component is defined by a spectral shape that contains a more rounded, slightly V-shaped ~800 to 1200 cm^{-1} region absorption. The low wavenumber absorption is uniform with no discernible minor absorptions. A rise in emissivity is present at wavenumbers just larger than 500 cm^{-1}. There is also a spectral shape that is intermediate between the first two types and may be considered a mixture of the two.

The shape, depth, and wavelength of the types 1 and 2 martian surface spectra are similar to spectra of several volcanic compositions (Fig. 2). The type 1 spectral shape is similar to a spectrum of a Deccan Traps flood basalt. This sample is composed primarily of plagioclase (~65 vol. %) and clinopyroxene (~30 vol. %) (*14*). The martian spectral shape also compares well with other basalt [45 to 52 weight % SiO_2 (45–52 wt. % SiO_2)] to low silica basaltic andesite (52–57 wt. % SiO_2) samples that are dominated by plagioclase and clinopyroxene mineralogies (*11*, *14*, *20*). The type 2 spectral shape is similar to that of a sample of basaltic andesite or andesite (the composition is on the border between the two fields at 57% SiO_2) composed primarily of plagioclase (~45 vol. %), potassium-rich (similar to obsidian) glass (~40 vol. %), and pyroxene (~10 vol. %) (*20*, *21*). Typical high-silica basaltic andesite to andesite (the term andesite is used here to mean an intermediate volcanic rock with 57–63 wt. % SiO_2) samples that are dominated by plagioclase and volcanic glass also compare well with the type 2 spectrum (*11*, *20*). Of the ~300 laboratory rock spectra examined for comparison, including igneous rocks of a wide variety of compositions as well as a broad suite of sedimentary and metamorphic rocks, no other compositions could be matched to either of the end-member spectra.

Modal mineralogies of the two martian spectral types were obtained with a least-squares fit of 45 mineral spectral end-members (*22*). The spectral end-members were selected to cover a wide range of mineral classes, including silicates, carbonates, sulfates, and oxides (*23*), and are similar to the mineral spectral set used by Christensen *et al.* (*3*). A blackbody spectrum (emissivity of unity at all wavelengths) was also included to account for possible differences in spectral contrast due to physical variations such as surface roughness between the mineral end-members and the martian surface (*24*, *25*). No continuum removal was applied at any point in the analysis.

Deconvolution results indicate that the

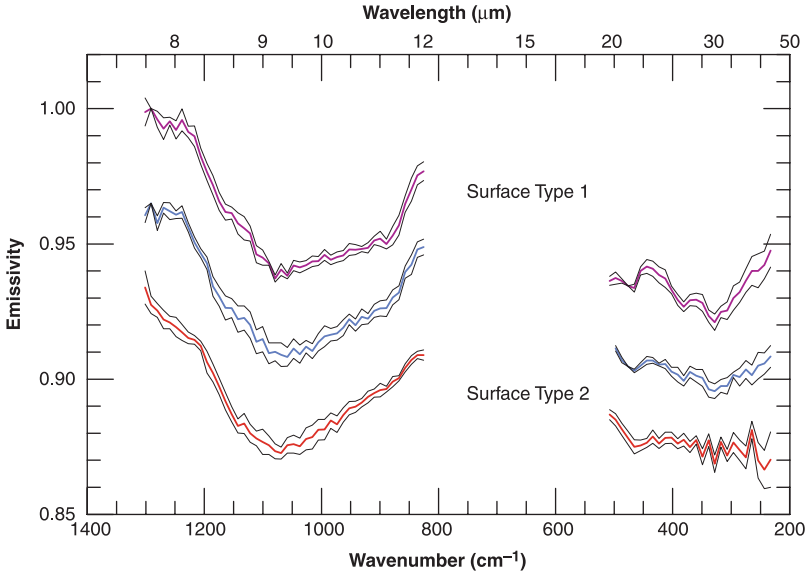

Fig. 1. Atmospherically corrected surface spectral types (offset by 0.04 for clarity). Each spectrum is an average of four to seven regional locations. Type 1 (top) is characteristic of Cimmeria, type 2 (bottom) is characteristic of Acidalia Planitia, and the intermediate type (middle) is characteristic of Sinus Meridiani. Thin lines denote the standard deviation for each sample and spectral shape.

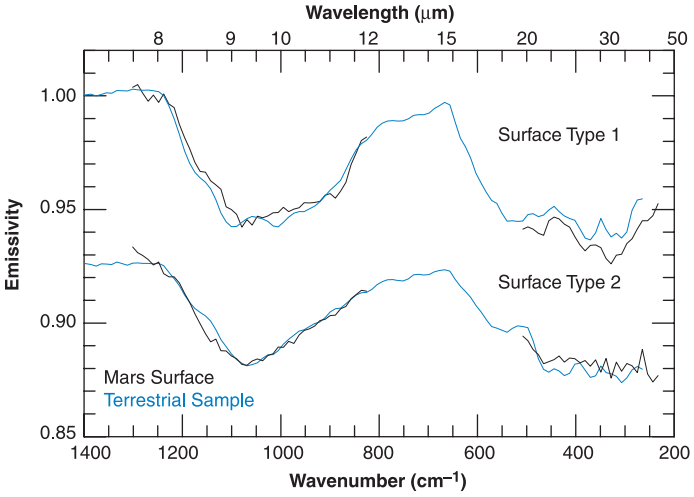

Fig. 2. Direct comparison of the two end-member surface types (black) (each type is offset by 0.07) with laboratory emissivity spectra of terrestrial particulate samples (cyan). Type 1 (top) is compared with a terrestrial basalt and type 2 (bottom) is compared with a terrestrial basaltic andesite–andesite. Shape depth and wavelength of absorption features match well to the terrestrial samples, which are sand-sized particulates. No contrast enhancement or continuum removal has been applied to any of the spectra.

type 1 spectrum is composed primarily of feldspar (predominantly plagioclase) and clinopyroxene (predominantly augite) (Fig. 3 and Table 1). These mineral concentrations are consistent with the results of Christensen *et al.* (*3*) for an atmospherically corrected spectrum from the Terra Cimmeria region. The deconvolution results for surface spectral type 2 indicate a surface composed of feldspar (predominantly plagioclase) and volcanic glass (*26*) (Fig. 3 and Table 1). Sheet silicates as well as clinopyroxene are present at or below the detection limit for both surface types. Other minerals were modeled at concentrations of ≤5%. These percentages are well below the detection limit, and the model fit did not degrade significantly [average root mean squared (RMS) error of 0.0028 versus 0.0022] when only the mineral classes listed in Table 1 were included in the spectral endmember set for deconvolution (*27*).

Sheet silicates (such as clays and micas) were identified for both martian surface types at concentrations of ~15%. However, these concentrations are at the detection limit of the technique, and it is difficult to discern which of the spectrally similar sheet silicates may be present. In addition, the derived concentration may represent an upper limit for the abundance of weathering products. Sheet silicates are often identified at similar concentrations in spectra of terrestrial rock samples that have only undergone minor weathering. Because weathering occurs primarily on the exterior surfaces and interior grain boundaries, spectra of exposed and fractured surfaces will show higher concentrations relative to their true volumetric abundance. This effect has been confirmed with laboratory spectra of cut surfaces that have significantly lower (<3% versus 10%) spectrally derived concentrations of weathering products (*11*). We conclude that sheet silicate weathering, if present, probably makes up a small fraction of the martian surface material in dark regions.

The deconvolution percentages represent areal coverage, and surface coatings such as weathering products may display a much higher areal abundance than the true volume abundance of the surface material. Although the sheet silicates may represent 15% of the surface area, the actual abundance of sheet silicates may be ≪1% by volume. The volume abundances of primary minerals will, as a result, be higher than the concentrations retrieved from the deconvolution.

The two spectral types, the hematite spectral shape (*4*), and the dust and water-ice spectral shapes (*1*) were used to fit ~10^7 individual TES emissivity spectra from the MGS mapping orbit dataset from heliocentric longitude (L_s) 103 to 247 (Northern Hemisphere summer through fall). This method calculates surface unit concentrations with a linear least-squares fitting routine similar to that used for retrieving mineral concentrations as described above (*28*). The concentrations of the two spectral types retrieved from the individual TES emissivity spectra were binned at 1° by 1° intervals to provide the regional distribution of these materials (Fig. 4). Surface spectral type 1 (basaltic) is concentrated primarily in southern highlands regions such as Terra Cimmeria and Noachis Terra with a large exposure in the Syrtis Major region as well. There are no significant (>25%) concentrations of surface type 1 in any Northern Hemisphere region outside of Syrtis Major. The distribution of spectral type 2 (andesitic) is distinct from that of spectral type 1. High concentrations are located primarily in the Northern Hemisphere in regions such as Acidalia Planitia, northwestern Syrtis Major, and Vastitas Borealis. There are several lower concentration exposures in the Southern Hemisphere in regions such as Sinus Meridiani and Margaritafer Terra. These exposures coincide with exposures of surface type 1 and represent locations where the two surface types are either mixed or the composition is intermediate between that of the two surface spectral types.

The RMS error image does not show any regions with large errors (>0.02) that may be attributed to a poor spectral fit. The RMS error is anticorrelated with signal to noise, which is dependent on surface temperature. As a result, RMS error is generally highest near the northern and southern borders of coverage as well as the generally colder high-albedo regions such as Hellas basin. The surfaces of all major regions covered to date by TES may be modeled with the two surface compositions and hematite.

The atmospherically corrected spectra and distribution maps indicate the presence of two distinct compositions in low-albedo regions on Mars. The ability to model all major low-albedo regions of Mars with only the two types of spectra and hematite indicates that there are no large concentrations of other surface compositions present on a regional scale.

It is possible that smaller exposures, such as exposures of bedrock in local areas like the walls of Valles Marineris, may be composed of different compositions; however, the two surface spectral types may account for the regional low-albedo exposures. Large exposures with martian meteorite-like compositions were not identified in any TES spectra of the surface, though with the exception of the shergottites, their cumulate nature and impact origin imply a deeper source that might not be widely distributed at the surface. Unfortunately, the source location for the martian meteorites is also missing. There are also no large exposures of other compositions such as komatiites, which have been proposed for Mars (*3*, *29*) and are more common in the ancient terrestrial rock record on Earth. Small exposures (≲20 km) of different compositions or slight variations in composition, such as low concentrations of additional minerals or compositional variations in existing minerals, may remain undetected.

Many martian low-albedo regions have thermal inertias (*17*, *30*, *31*) as well as the spectral contrast (*3*) (Fig. 2) expected for sand-sized particles. As a result, the intermediate spectral shape may represent a physical mixture of the first two compositions rather than an intermediate composition. Determining the sources of these sands may be difficult, as

Table 1. Mineral areal percentages retrieved by deconvolution for both surface endmember spectral shapes (*23*). Minerals in parentheses indicate concentrations at or below detection limit (~10 to 15%).

Surface type 1	Concentration (%)	Surface type 2	Concentration (%)
Feldspar*	50	Feldspar	35
Clinopyroxene†	25	Glass	25
(Sheet silicates)	15	(Sheet silicates)	15
		(Clinopyroxene)	10

*Plagioclase is the dominant feldspar. †Augite is the dominant clinopyroxene.

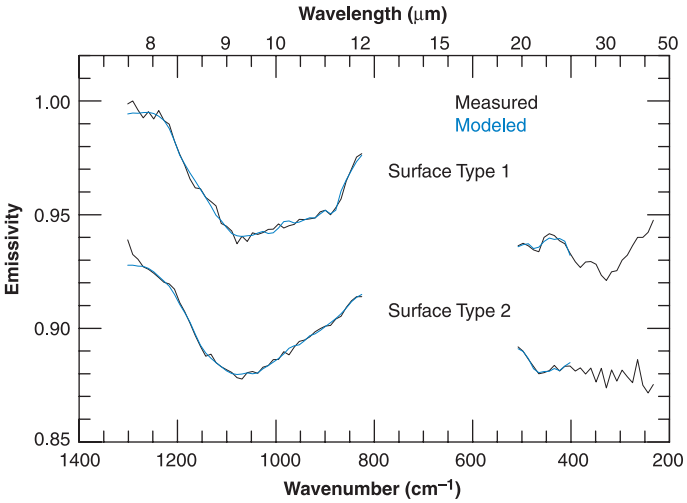

Fig. 3. Martian surface spectra (black) and deconvolution model spectra (cyan) (Table 1). Surface type 1 (top) and type 2 (bottom) are both modeled within 0.002 RMS error, and all spectral features are matched well.

outflow channels that originate in the southern highlands may be the source for the relatively high silica materials in Acidalia and Vastitas Borealis. However, it is unlikely that the hemisphere-scale compositional differences are solely due to transport processes (*32*). Surface composition probably represents local or regional bedrock composition.

Distributions of the surface spectral types are split roughly along the planetary dichotomy that separates the ancient heavily cratered crust of Mars from the younger northern plains. The basaltic composition is restricted to southern highlands and Syrtis Major regions that are of Noachian or Hesperian age. The more silicic composition displays the highest concentrations in the younger Amazonian-age northern lowlands. Intermediate compositions or lower concentrations of the andesitic unit are also common in the southern highlands.

If the low-albedo surface materials are locally or regionally derived, they indicate that basaltic volcanism has been restricted to the more distant past. Andesitic volcanism appears to have occurred throughout much of Mars's history but is more dominant than basaltic volcanism in more recent times. This progression suggests an increased evolution of martian lavas with time. The mechanisms or events that led to the formation of the planetary dichotomy may also have a link to the change in volcanic compositions on Mars.

The two surface end-members represent two distinct compositions that occur commonly on Earth. Crystalline basalt to low-silica basaltic andesite, which requires no major differentiation beyond partial melting of the mantle, is common in hot-spot, flood volcanism, and rifting environments. This composition does not represent highly evolved, differentiated, or cumulate compositions such as the lunar basalts or martian meteorites [summarized in (*33, 34*)]. Glassy, high-silica basaltic andesite to andesite requires more differentiation than basalts that may be due to silica enrichment as a result of higher water contents, cumulate formation, and/or repeated partial melting (*34–36*). Although on Earth, this type of volcanism is most commonly associated with plate subduction (for which there is no evidence on Mars), smaller volumes of andesitic lavas are produced in a variety of environments on Earth (*36*).

The presence of 35 to 50% feldspar concentrations in both spectral types indicates that the alumina content of these surface materials is higher than that observed in most of the martian meteorites (*33, 36*) and in the elemental soil analyses returned from the Viking x-ray fluorescence (*37*) and Pathfinder Alpha Proton X-ray Spectrometer (APXS) experiments (*38*). High feldspar contents are more consistent with, and perhaps exceed, the relatively high alumina content derived for the sulfur-free rock at the Pathfinder landing site (*36*, *38*). The relatively high silica content of the clast deposits at the Pathfinder landing site are also consistent with the composition of the andesitic surface type observed by the TES instrument in the same region.

Previous spectroscopic studies have identified variable ~1- and 2-μm absorptions attributed to the presence of pyroxene in low-albedo regions (*39–42*). These absorptions are not ubiquitous, however, as there is no apparent ≳1 μm Fe^{2+} absorption present in telescopic spectra of Acidalia Planitia (*43*) or in the 12-point spectra of rocks at the Pathfinder landing site (*36*). Pyroxene compositions in the surface type 1 (basaltic) are consistent with that of an average composition of augite in Imaging Spectrometer for Mars (ISM) near-infrared spectral data analyzed by Mustard *et al.* (*42*) in the Syrtis Major region. In regions where there is a glass component from surface type 2 (andesitic) in addition to clinopyroxene from surface type 1, pyroxene concentrations are too low to obtain a precise high Ca to low Ca ratio with TES data. Large glass concentrations and the lack of orthopyroxenes in surface type 2 agree with the lack of distinct Fe^{2+} absorptions short of ~1 μm in reflectance spectra of Acidalia (*43*) and at the Pathfinder landing site (*36*).

Similar to both the Earth's ocean basins and continents and the moon's mare and highlands, Mars also displays a dichotomy in global composition with two distinct geologic terrains. These compositions are similar to those of typical basalts and andesites on Earth, the two most common volcanic types, which implies that the same bulk volcanic compositions and conditions were present on both planets. However, the apparent lack of subduction-related volcanism raises the question of what processes have led to widespread andesitic volcanism on Mars.

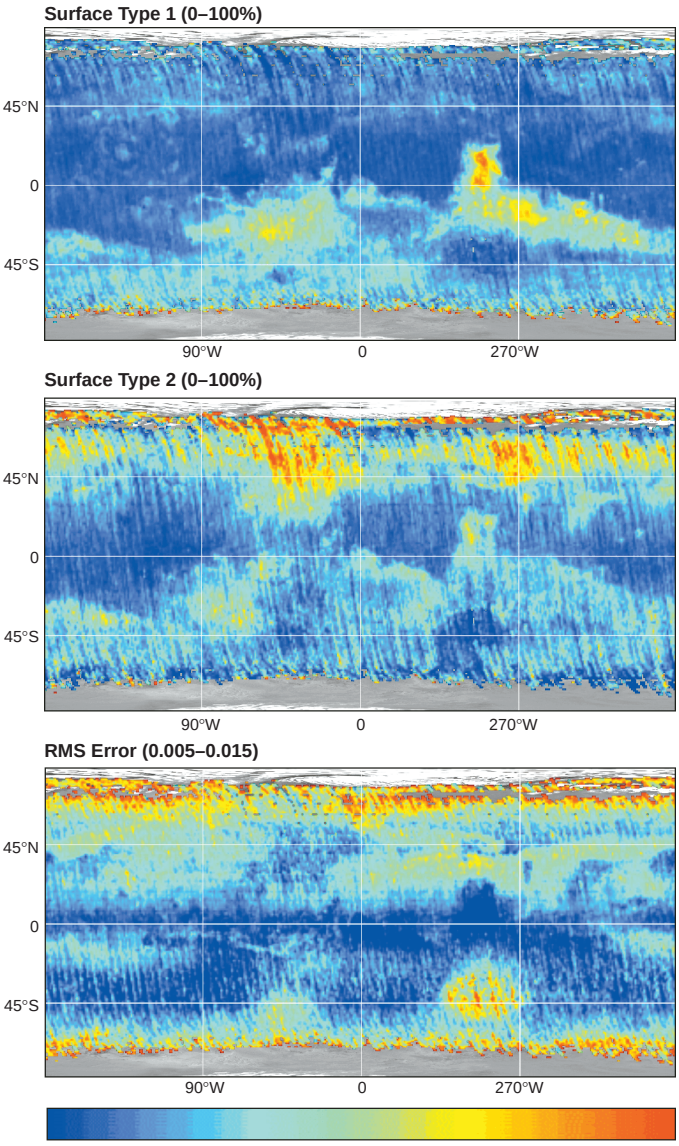

Fig. 4. Global areal concentrations of the two surface types and the RMS error image overlaid on a global albedo map. Ranges in parentheses give the lowest unit (blue) to the highest unit (red) on the scale bar. The extent of the polar cap in the Southern Hemisphere during the initial mapping phase prevented the acquisition of data south of ~70°S.

References and Notes

1. J. L. Bandfield, P. R. Christensen, M. D. Smith, *J. Geophys. Res.* in press.
2. M. D. Smith, J. L. Bandfield, P. R. Christensen, *J. Geophys. Res.* in press.

3. P. R. Christensen, J. L. Bandfield, M. D. Smith, V. E. Hamilton, *J. Geophys. Res.*, in press.
4. P. R. Christensen *et al.*, *J. Geophys. Res.*, in press.
5. M. D. Smith, J. C. Pearl, B. J. Conrath, P. R. Christensen, *J. Geophys. Res.*, in press.
6. The TES instrument is a Fourier transform Michelson interferometer that covers the wavenumber range from 1700 to 200 cm^{-1} (~6 to 50 μm) at 10 cm^{-1} or 5 cm^{-1} sampling [P. R. Christensen *et al.*, *J. Geophys. Res.* **97**, 7719 (1992)]. The instrument also contains bore-sighted thermal (5 to 100 μm) and visible/near-infrared (VNIR) (0.3 to 3.5 μm) bolometers. The focal planes for the interferometer and the bolometers consist of three cross-track and two along-track detectors with an instantaneous field of view (IFOV) of ~8.5 mrad. The TES instrument uses a pointing mirror that allows for limited targeting capability, limb observations, image motion compensation (IMC), and periodic calibration by observing space and an internal reference surface. The final 2-hour circular mapping orbit of MGS provides a continuous data strip three pixels wide with a spatial sampling of ~3 km by 9 km from a mean altitude of 379 km. The elongated pixel dimension is due to the final mapping orbit of MGS, which crosses the equator at ~2 a.m. local time rather than the intended ~2 p.m. because of damage to the spacecraft solar panel that required lower aerobraking rates. Spacecraft direction relative to the surface is reversed, and IMC does not produce adequate results when stepping the mirror in a direction opposite that originally intended. As a result, spatial sampling is smeared in the along-track direction. These data have improved regional coverage, spatial resolution, and radiometric precision over the aerobraking and science phasing data because of the characteristics of the final MGS 2 p.m. mapping orbit.
7. Christensen *et al.* (*3*) provide a detailed analysis of the uncertainties in atmospherically corrected spectra. For a 280 K surface, the total error in emissivity from random and systematic sources before atmospheric correction is <0.0013 from 300 to 1100 cm^{-1}, increasing to 0.0035 at 1400 cm^{-1} for an average of all six detectors. Random error is lower in the averaged spectra presented here, reducing these uncertainties somewhat. Error due to the atmospheric correction was estimated and is similar to the errors shown in Fig. 1.
8. R. J. P. Lyon and E. A. Burns, *Econ. Geol.* **58**, 274 (1963).
9. G. R. Hunt and J. W. Salisbury, *Environ. Res. Pap. 496-AFCRL-TR-74-0625* (1974).
10. J. W. Salisbury, L. S. Walter, D. D'Aria, *U.S. Geol. Surv. Open-File Report 88–686* (1988).
11. K. C. Feely and P. R. Christensen, *J. Geophys. Res.* **104**, 24195 (1999).
12. M. S. Ramsey and P. R. Christensen, *J. Geophys. Res.* **103**, 577, (1998).
13. M. S. Ramsey, P. R. Christensen, N. Lancaster, D. A. Howard, *Geol. Soc. Am. Bull.* **111**, 646, (1999).
14. V. E. Hamilton and P. R. Christensen, *J. Geophys. Res.*, in press.
15. A. R. Gillespie, *Remote Sensing Environ.* **42**, 137 (1992).
16. J. L. Thomson and J. W. Salisbury, *Remote Sensing Environ.* **43**, 1 (1993).
17. F. D. Palluconi and H. H. Kieffer, *Icarus* **45**, 415, (1981).
18. P. R. Christensen, *J. Geophys. Res.* **87**, 9985 (1982).
19. ———, *J. Geophys. Res.* **103**, 1733 (1998).
20. M. B. Wyatt *et al.*, in preparation.
21. The sample and petrologic analysis were provided by M. B. Wyatt. The glass composition is consistent with rhyolite obsidian with ~75% SiO_2.
22. The least-squares fit algorithm is an iterative program that successively removes concentrations that are less than zero and, therefore, unrealistic. This iterative process may only find a local, rather than global, minimum. Although this raises the possibility of inaccuracies, Feely and Christensen (*11*) and Hamilton and Christensen (*14*) have applied this method extensively and found no adverse or systematic defects due to the iterative process. An additional modification to this algorithm reruns the iterative least-squares fit with only spectral classes found in the final iteration of the algorithm. For example, if the final iteration contains positive concentrations of only diopside and andesine, the algorithm is run again with an end-member set that includes all feldspars and clinopyroxenes that are spectrally similar to andesine and diopside but excludes all other mineral spectra. This commonly improved the fit and reduces the possibility that a correct end-member is accidentally thrown out in the iterative process. The mineral end-member set is currently limited to 400 cm^{-1} and, as a result, the analysis was not performed between 200 and 400 cm^{-1}.
23. Most of the minerals used are from P. R. Christensen *et al.*, *J. Geophys. Res.*, in press. For a complete list, see the supplemental data available at *Science* Online at www.sciencemag.org/feature/data/1047493.shl.
24. V. E. Hamilton, P. R. Christensen, H. Y. McSween Jr., *J. Geophys. Res.* **102**, 25593 (1997).
25. M. S. Ramsey and J. H. Fink, *Bull. Volcanol.* **61**, 32 (1999).
26. The glass end-member used in the analysis is an rhyolite obsidian with a high silica (74% SiO_2) content (*25*).
27. Christensen *et al.* (*3*) performed a similar analysis on a surface spectrum from Terra Cimmeria to test the confidence of minor mineral percentages (<15%).
28. The spectra used were limited to surfaces warmer than 245 K, dust extinctions of <0.25, ice extinctions of <0.15, and RMS fits of measured to modeled spectra of <0.03. Because of the computationally extensive nature of temperature profile retrieval, dust and water-ice opacities were unavailable at the time of analysis. However, although opacity does not correlate perfectly with extinction, low extinctions will limit opacity for surfaces warmer than the atmosphere. Limiting the RMS error of the least-squares fit provides a quick method for filtering highly anomalous data due to errors such as lost bits, mislabeled calibration pairs, and compression errors. These criteria are less restrictive than those used to retrieve the spectral types because the fitting routine is more constrained with fewer end-members. TES emissivity spectra of warm surfaces under a variety of atmospheric and topographic conditions may be modeled with only dust, water-ice, and surface spectral shapes (*1*). While this only provides extinctions, rather than opacities, of atmospheric components, concentrations of each of the surface spectral units may be retrieved (*2*).
29. D. P. Reyes and P. R. Christensen, *Geophys. Res. Lett.* **21**, 887 (1994).
30. H. H. Kieffer *et al.*, *J. Geophys. Res.* **82**, 4249 (1977).
31. M. A. Prestley and P. R. Christensen, *J. Geophys. Res.* **102**, 6551 (1997).
32. C. Sagan, D. Pieri, P. Fox, R. E. Arvidson, E. A. Guinness, *J. Geophys. Res.* **82**, 4430 (1977).
33. H. Y. McSween Jr., *Meteoritics* **29**, 757 (1994).
34. Basaltic Volcanism Study Project, *Basaltic Volcanism on the Terrestrial Planets*, (Pergamon, New York, 1981).
35. J. Gill, *Orogenic Andesites and Plate Tectonics* (Springer-Verlag, New York, 1981).
36. H. Y. McSween Jr. *et al.*, *J. Geophys Res.* **104**, 8679 (1999).
37. P. Toulmin *et al.*, *J. Geophys. Res.* **82**, 4625 (1977).
38. R. Rieder *et al.*, *Science* **278**, 1771 (1997).
39. J. B. Adams and T. B. McCord, *J. Geophys. Res.* **74**, 4851 (1969).
40. R. B. Singer, *Proc. Lunar Planet. Sci. Conf.* **11**, 1048 (1980).
41. R. B. Singer and H. Y. McSween Jr., in *Resources of Near Earth Space*, J. Lewis, M. S. Matthews, M. L. Guerrieri, Eds. (Univ. of Arizona Press, Tuscon, AZ, 1993), pp. 709–736.
42. J. F. Mustard *et al.*, *J. Geophys. Res.* **98**, 3387 (1993).
43. E. Merenyi, R. B. Singer, J. S. Miller, *Icarus* **124**, 280 (1996).

44. We thank H. Moncrief, N. Gorelick, S. Anwar, K. Bender, K. Feely, K. Homan, and G. Mehall for software and operations support and M. Kraft, M. Smith, J. Pearl, W. Stefanov, S. Ruff, M. Wyatt, H. McSween, R. Morris, and J. Holloway for valuable discussions of the results presented here. We also thank the dedicated spacecraft and operations teams at Jet Propulsion Laboratory and Lockheed Martin.

30 November 1999; accepted 19 January 2000

Isotope Fractionation and Atmospheric Oxygen: Implications for Phanerozoic O_2 Evolution

R. A. Berner,[1] S. T. Petsch,[1] J. A. Lake,[2] D. J. Beerling,[2] B. N. Popp,[3] R. S. Lane,[3] E. A. Laws,[3] M. B. Westley,[3] N. Cassar,[3] F. I. Woodward,[2] W. P. Quick[2]

Models describing the evolution of the partial pressure of atmospheric oxygen over Phanerozoic time are constrained by the mass balances required between the inputs and outputs of carbon and sulfur to the oceans. This constraint has limited the applicability of proposed negative feedback mechanisms for maintaining levels of atmospheric O_2 at biologically permissable levels. Here we describe a modeling approach that incorporates O_2-dependent carbon and sulfur isotope fractionation using data obtained from laboratory experiments on carbon-13 discrimination by vascular land plants and marine plankton. The model allows us to calculate a Phanerozoic O_2 history that agrees with independent models and with biological and physical constraints and supports the hypothesis of a high atmospheric O_2 content during the Carboniferous (300 million years ago), a time when insect gigantism was widespread.

A dominant feature of Earth's atmosphere is the presence of abundant free oxygen (O_2), which signifies an active aerobic biosphere. Much attention has been directed toward understanding the rise of O_2 during the Precambrian (*1–5*). Of equal interest, however, is the relative lack of